RESEARCH ARTICLE

Controlling factors of phytoplankton distribution in the river–lake transition zone of a large lake

Gabriel Cotte[1] · Frédéric Soulignac[2,4] · Fabio dos Santos Correia[3] · Matthieu Fallet[1] · Bastiaan Willem Ibelings[3] · David Andrew Barry[2] · Torsten W. Vennemann[1]

Abstract

River–lake transition zones have been identified as major drivers of phytoplankton growth. With climate change reducing the frequency of complete lake overturns, it is expected that the Rhône River, the main tributary to Lake Geneva (France/Switzerland), will become the major source of nutrients for the lake euphotic zone. The river–lake transition zone was hence examined at the mouth of the Rhône River with the aim of understanding the complexities and controls of phytoplankton distribution in this specific deltaic ecosystem. Two field campaigns were carried out in which water samples were collected from longitudinal and transversal transects across the transition zone. These samples were analyzed for both nutrient and phytoplankton concentrations, while the fraction of Rhône River water in a lake sample was determined by the stable isotope composition of the water. The results indicate contributions in P and Si related to the Rhône intrusion into the lake. Furthermore, this river–lake transition zone appears to be a dynamic area that can locally present optimal conditions for phytoplankton growth. In early spring, a wind event broke the early and weak stratification of the lake, forcing the Rhône River and its turbidity plume to intrude deeper. Thus, this sharp drop of the turbidity within the euphotic zone allowed an increase in the phytoplankton biovolume of 44%. In early fall, outside of the turbid near field of the river mouth, the Rhône interflow, located just below the thermocline, promoted a local deep chlorophyll maximum.

Introduction

Large lakes of the world are habitats for diverse species and represent resources for humanity by providing many ecosystem services (Sterner et al. 2020). Yet, these ecosystems are experiencing rapid degradation as they are exposed to anthropogenic and climatic stressors (e.g., Jenny et al. 2020). One of the most common threats faced by large lakes is eutrophication (Richardson and Jørgensen 2013), characterized by recurrent algal blooms and deep-layer hypoxia

✉ Gabriel Cotte
  gabriel.cotte@protonmail.com

  Frédéric Soulignac
  f.soulignac@cipel.org

  Fabio dos Santos Correia
  fabio.dossantoscorreia@unige.ch

  Matthieu Fallet
  fallet.matthieu@gmail.com

  Bastiaan Willem Ibelings
  bastiaan.ibelings@unige.ch

  David Andrew Barry
  andrew.barry@epfl.ch

  Torsten W. Vennemann
  torsten.vennemann@unil.ch

[1] Institute of Earth Surface Dynamics (IDYST), University of Lausanne (UNIL), 1015 GéopolisLausanne, Switzerland

[2] Ecological Engineering Laboratory (ECOL), Institute of Environmental Engineering (IIE), School of Architecture, Civil and Environmental Engineering (ENAC), Ecole Polytechnique Fédérale de Lausanne (EPFL), 1015 Lausanne, Switzerland

[3] Department F.-A. Forel for Environmental and Aquatic Sciences (DEFSE) and Institute for Environmental Sciences (ISE), University of Geneva (UNIGE), Uni Carl Vogt, 1205 Geneva, Switzerland

[4] Present Address: Commission Internationale Pour la Protection des eaux du Léman, Route de Duillier 50, 1260 Nyon, Switzerland

(Jenny et al. 2016). The abundance of phytoplankton within lakes has been recognized as an important component of their water quality management (Xu et al. 2001). However, understanding phytoplankton dynamics in large lakes poses many challenges, including taking into account their highly heterogeneous distribution (Ghadouani and Smith 2005; Viljanen et al. 2009; Leoni et al. 2014).

Recently, several studies have been conducted to better understand the spatio-temporal heterogeneities of phytoplankton abundance in large lakes. Dynamics of algal growth can be explained by temporal and spatial variability in thermal stratification dynamics and internal wave motions (Yang et al. 2016; Soulignac et al. 2018). Furthermore, a higher abundance of phytoplankton has been reported around river inflow areas (Larson et al. 2013; Kiefer et al. 2015; Soomets et al. 2019). Another factor affecting the phytoplankton dynamics of lakes is climate change, which extends the growing season with an earlier onset of stratification and associated earlier algal blooms in spring (Anneville et al. 2018; Woolway et al. 2021). Moreover, climate warming is expected to reduce the frequency of complete lake overturns occurring at the end of winter in monomictic lakes, a process that brings bottom nutrients to the surface water (Perroud et al. 2009; Woolway and Merchant 2019). Consequently, it is expected that other sources of nutrient to the euphotic zone, such as nutrients coming from the watershed, will have a more pronounced impact on phytoplankton distribution (Anneville et al. 2013). It is then important to further evaluate the riverine inputs of the nutrients, their transport and their subsequent distribution in lakes, to help understand their metabolization and hence their role in the primary production of lakes.

Chemical and biological gradients in the receiving lake are usually associated with river inflows (Schelske et al. 1980; Morrice et al. 2004; Makarewicz et al. 2012). These transition zones are defined as regions where hydrodynamic conditions transform from river-dominated flow to lake mixing processes (Thornton 1990). The differences in water density between the river and the receiving lake, together with the mixing processes, control the river intrusion pattern within the transition zone and determine the bioavailability of the river nutrients for phytoplankton (Rueda et al. 2007). On the one hand, if the river water is less dense than the lake water, the river water carrying the nutrients is transported as an overflow, and resources will be directly bioavailable in the surface layer. On the other hand, if the river water is denser than the lake water surface, as it is generally the case for the Rhône River in Lake Geneva, it will plunge and be distributed as an underflow. The river can flow down to the lakebed or can intrude into the water column when it reaches the depth of neutral buoyancy and generate an interflow (Fig. 1). Depending on this intrusion depth, the river nutrients can directly fuel algal growth if they are inserted within the euphotic zone, where the primary production takes place, or indirectly, if the intrusion occurs below the euphotic zone but nutrients are transported upwards by vertical mixing. Consequently, hydrodynamic processes occurring in the river–lake transition zone determine the chemical and biological gradients. Despite the commonly accepted importance of the river–lake transition zones in lacustrine ecosystems (Mackay et al. 2011; Makarewicz et al. 2012; Larson et al. 2016), the link between the hydrodynamic processes, the physico-chemical properties of the lake and the phytoplankton distribution in these transition zones is infrequently studied in large lakes.

Preliminary field measurements (results unpublished) made during July 2018 showed a high concentration of chlorophyll *a* (Chl *a*) and phytoplankton close to the Rhône River mouth in Lake Geneva suggesting an optimal zone for phytoplankton growth where an equilibrium occurs between the nutrients transported by the Rhône River and the other limiting factors within the lake, such as sunlight

Fig. 1 Conceptual model of a negatively buoyant inflow entering a stratified lake. After plunging, the river inflow can intrude into the water column when it reaches the depth of neutral buoyancy and generate an interflow. The river mouth near field is defined as the area where the river current velocity is still measurable
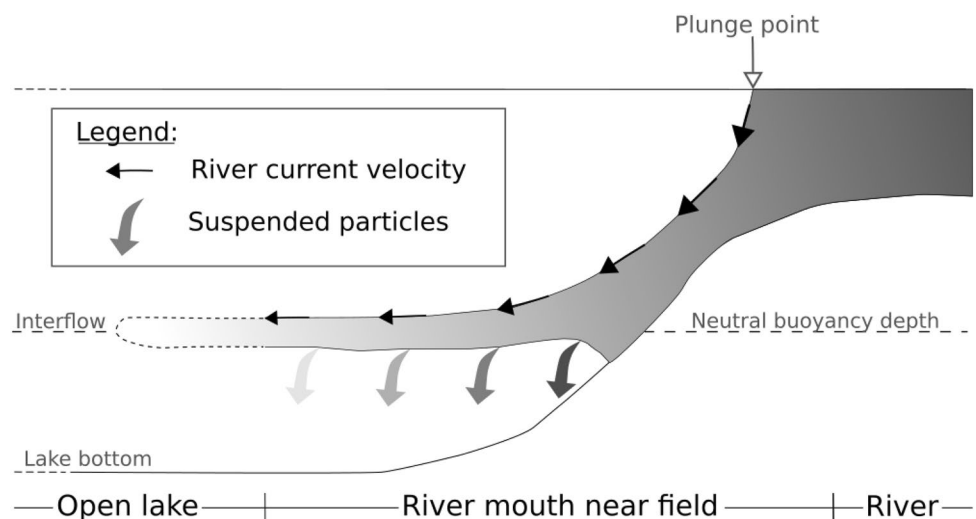
(low turbidity), low flow speed and temperature. Field experiments within a 2 km radius from the river mouth revealed complex hydrodynamics in this region, involving the introduction and subsequent loss of suspended sediments in the river–lake transition zone (Piton et al. 2022). Moreover, we presume that some hydrodynamic processes occurring at the river mouth, such as sudden changes in the river intrusion depth (Soulignac et al. 2021), may modify the conditions for phytoplankton growth. Overall, these initial measurements support the existence of an ecocline in the Rhône River–Lake Geneva transition zone as typically observed in estuarine environments (Attrill and Rundle 2002). An ecocline can be defined as a gradual ecological boundary between two systems related to the progressive change of a major environmental factor (van der Maarel 1990).

Chemical and biological gradients occurring in river–lake transition zones have been studied widely (Schelske et al. 1980; Marti et al. 2011; Jameel et al. 2018; Carlson Mazur et al. 2019). However, this is the first time that a study couples hydrodynamic and physico-chemical measurements to explain the phytoplankton distribution in the river discharge zone of a large lake. With this aim, our specific research questions are:

1) Are there significant nutrient contributions related to the Rhône River intrusion into the river–lake transition zone?
2) Which hydrodynamic processes in the transition zone, if any, affect the conditions for phytoplankton growth?
3) Is there a biological gradient, or in other words, is there a specific ecocline present in this transition zone?

Materials and methods

Study site

Lake Geneva (local name: *Lac Léman*) is a large and deep monomictic lake located in the western part of the Alps, on the border between France and Switzerland. After a period of eutrophication during the 1960s and 1970s with annual average total phosphorus concentrations reaching 90 µg P/L, phosphorus input into the lake has been limited due to Swiss and French measures taken since the 1980s, leading to a decrease in total phosphorus to about 16 µg P/L in 2019 (CIPEL 2020). Since 1995, phosphorus (P) is the limiting nutrient for primary production, while silica (Si) influences the phytoplankton succession with the replacement of diatoms by non-siliceous species (Moisset 2017).

The Rhône River is the principal tributary to Lake Geneva, both in terms of discharge of water and sediment load. It represents 77% of the annual dissolved inorganic phosphorus riverine input into the lake (24 t in 2018, CIPEL 2019). Therefore, it influences the physical and chemical properties of the lake and also its ecological functioning (Bouffard and Perga 2016; Nouchi et al. 2019). The mouth of the Rhône River is located in the eastern part of Lake Geneva, called the *Haut Lac* (Fig. 2). The *Haut Lac* is part of the eastern main basin of Lake Geneva, called the *Grand Lac*, with the smaller *Petit Lac* lying to the west. It was shown that during the lake-stratified period, from spring to early fall, the Rhône River intrudes the lake water column at the level of neutral buoyancy as an interflow (Halder et al. 2013). This interflow occurs at the depth of the thermocline and it is transported through the entire lake metalimnion by the circulation gyres of the lake (Cimatoribus et al. 2019; Cotte and Vennemann 2020). During occasional high discharge events when the Rhône River carries a high sediment load, the river inflow breaks through the thermocline and flows as a turbidity current through a subaquatic canyon, carrying its nutrients down into the deep hypolimnion (Loizeau and Dominik 2000; Kremer et al. 2015; Corella et al. 2016). Lake Geneva water quality is monitored at two stations: SHL2 at the deepest point of the *Grand Lac*, and GE3 in the *Petit Lac* (CIPEL reports 1969 to 2020).

Sampling strategy

Fieldwork included two seasons: the first campaign was in April during the spring phytoplankton bloom, which also represents the period of the onset of the thermal stratification of Lake Geneva, and a second campaign in September at the end of summer covering a period of stronger stratification with a euphotic zone being more depleted in dissolved nutrients (CIPEL 2020). Two transects were sampled per campaign, each campaign covering two days, with one transect per day (Fig. 2). The transversal transect (T1) was located in the near field where the momentum-dominated initial river discharge transitions into a buoyancy-forced plume (Fig. 1). In this study, the near field is defined as the area where the Rhône interflow current velocity is still measurable with a typical background current in the lake of 10 cm/s. The second, longitudinal transect (T2) goes from the river mouth to the open lake. The suffixes A for April and S for September were added to the transect names to differentiate the campaigns (e.g., T1-A, T1-S). The sampling stations of the transversal and the longitudinal transects were numerated with Roman and Arabic numeral, respectively (e.g., A-II, S-3). Details on the location and sampling date of the different sampling stations can be found in Table S1.

On 2 April 2019, the T2-A stations were chosen on the basis of the forecast of an online hydrodynamic model of Lake Geneva (http://meteolakes.ch, Baracchini et al. 2020). These simulations indicated lake water currents in the main basin deflecting the water towards the northern shore (Figure S1). One station was then placed 1 km in front of the Rhône
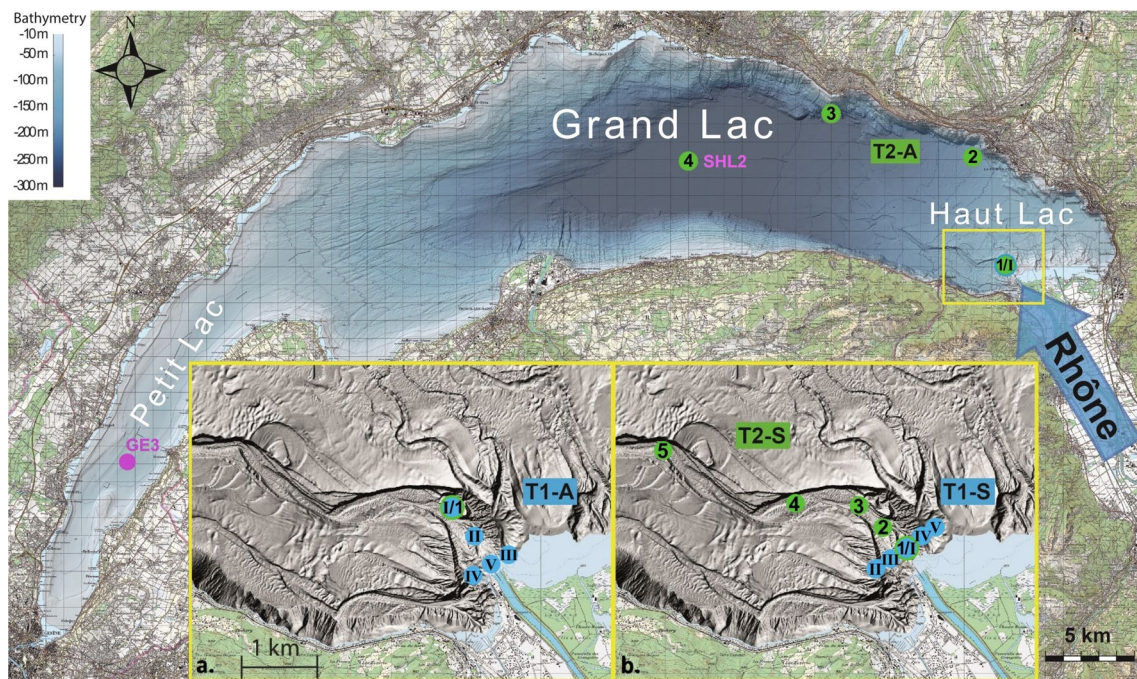
Fig. 2 Bathymetric map of Lake Geneva and sampling stations of transect T2 in April (1 to 4) (main map). The Rhône River inflow is indicated by a blue arrow. SHL2 and GE3, in purple, are the two permanent monitoring stations within Lake Geneva. Larger scale maps of the Rhône River mouth area show the sampling stations of transect

T1 in April (I to V) (insert a) and sampling stations of transect T1 (I–V) and T2 (1–5) in September (insert b). Station 1 corresponds to station I (1/I) for both seasons. Transects T1 are in blue and transects T2 are in green

River mouth (A-1) and two along the northern shore (A-2, 5 km and A-3, 14 km from the river mouth). An additional sampling station was placed 22 km from the river mouth, towards the middle of the lake (A-4), still on the predicted path of the Rhône interflow transported by the lake water currents and also corresponding to the location of the SHL2 monitoring station. On 4 April, because no trace of interflow was detected at 5 km from the river mouth (station Ib, Figure S2), the T1-A stations (I to V) were placed closer to the river mouth above the actual Rhône's canyon, with station A-I corresponding to station A-1 and station A-V located in the plunge zone.

On 24 September 2019, sampling covered stations I to V for T1-S and on 26 September, the stations 1–5 for T2-S (Fig. 2). Continuous vertical profiles of current velocity and direction were measured using an Acoustic Doppler Current Profiler (ADCP) along the rectilinear ADCP transect 1 corresponding to T1-S on the 24 September, and along the curvilinear ADCP transects 2–5 on the 26 September (Figure S3). The Teledyne Marine Workhorse Sentinel ADCP was mounted facing downwards on a small catamaran, which was towed by a boat at approximately 0.7 m/s. The bin size was set to 1 m and the number of bins to 100. The ADCP measurements were used to track the river interflow current along its development from the river mouth into the lake (Figure S3). Concerning the sampling stations of T1-S, station S-I

was located in the middle of the river interflow current measured on the rectilinear ADCP transect 1 at 400 m from the river mouth. Stations S-II and S-V were located west and east, respectively, at the edges of the river interflow current. Station S-III was located in the middle of stations S-II and S-I, and station S-IV was in the middle of stations S-I and S-V. The stations S-1 to S-3 were located in the center of the river interflow current at 400, 800 and 1200 m from the river mouth, respectively, with station S-1 corresponding to station S-I. Station S-4 marks the limit of the near field area at 2 km and station S-5 is the background station located 4 km from the river mouth.

Samples for the chemical and biological measurements were taken using an automatic Rosette water sampler (1018 Mini Rosette Sampling System, General Oceanics Inc.). The Rosette consists of 11 Niskin bottles (each 1.7 L) and was coupled to a CTD (Conductivity-Temperature-Depth) probe (OCEAN SEVEN 316Plus CTD, IDRONAUT Srl), which was externally powered via a telemetry cable to provide real-time information on electrical conductivity, oxygen, pH, temperature, turbidity and pressure (depth). A continuous CTD cast without interruption was taken while lowering the sampling system and water samples were taken when raising the system. To compare the different profiles, systematic depth sampling was chosen for the depth locations. Ten of the eleven bottles of the Rosette were used for this

sampling (1, 2.5, 5, 7.5, 10, 15, 20, 30, 100 m, bottom) and the remaining bottle to sample a possible peak of turbidity in the middle of the interflow. CTD data were saved when the water samples were taken. The sensor precisions are 0.003 mS/cm for conductivity, 0.003 °C for temperature, 0.05% for pressure, 0.001 units for pH, and 0.01 ppm for oxygen measurements. Conductivity [κ25] is given relative to 25 °C. Physical data were processed by REDAS-5 Release 5.40 (IDRONAUT Srl). For the biological analysis, 5 mL aliquots were taken directly from the raw water samples and fixed with 200 μL of glutaraldehyde (Vaulot et al. 1989). For the chemical analysis, water samples were filtered with 0.45 μm nylon filters using a peristaltic pump and stored at 5 °C directly on board. Upon return to the laboratory, samples were stored at − 18 °C until the major ion analysis was done. Split samples for the stable isotope analysis were refrigerated at 5 °C prior to analysis, performed within a week of sampling. Concerning the spatial uncertainties, the drift between the theoretical and the real sampling locations was evaluated by GPS. To solve this problem and minimize the error, two rules were established. First, sampling campaigns were cancelled if the wind speed was superior to 10 m/s. Secondly, if the drift was greater than 100 m during the sampling, the profiles were repeated. Additionally, an ISCO automatic sampler was installed at Porte du Scex, located 5 km upstream of the Rhône River mouth, which sampled the river water on a daily basis in parallel to the sampling campaigns to determine the daily fluctuations of the stable isotope composition. Finally, grab river samples were taken at the river mouth with a bucket from the river surface every sampling day to evaluate the nutrient input from the Rhône watershed.

Analysis

Stable water isotopes

The oxygen and hydrogen isotope compositions were analyzed using a Picarro L2140i following the method described by Cotte and Vennemann (2020). The uncertainty related to the analytic error calculated by the standard deviation of all repeated measurements was $\pm 0.05‰$ for oxygen and $\pm 0.2‰$ for hydrogen.

Nutrient concentrations

Orthophosphate ($P-PO_4^{3-}$) concentrations were measured spectrophotometrically using the molybdenum blue method (Murphy and Riley 1962) at 882 nm on a UV–visible spectrometer (Perkin Elmer). The analytical error was estimated by the standard deviation of the standards analyzed as triplicates. The detection limit is 0.5 μg ($P-PO_4^{3-}$)/L.

Nitrate concentrations were measured by liquid ion-chromatography (Dionex ICS-1100). Each sequence was calibrated using five standards. A sequence consisted of duplicate samples, internal standards and blanks. The analytical error for each sample was estimated by the standard deviation of the duplicates. The detection limit is 0.07 mg ($N-NO_3^{-}$)/L.

Silica concentrations were measured spectrophotometrically using a SmartChem 200 (AMS Alliance). Sample duplicates were analyzed with internal standards and blanks. The standard deviation of the duplicates was used to evaluate the analytical error. The detection limit is 0.1 mg SiO_2/L.

All the chemical analysis results are presented in Table S2.

Phytoplankton biovolume

A CytoSense scanning flow cytometer (CytoBuoy, The Netherlands) was configured with a smart-trigger level of 20 mV for red fluorescence (FLR, targeted to count only the particles having chlorophyll) at a flow rate of 4.1 μL/s for 15 min maximum; the pump switched off once 15,000 particles were analyzed. After a testing phase, data were treated with *CytoClus 4* software to remove electronic noise and any debris such as particulate organic matter. The measurements used for results included the concentration of phytoplankton [individuals/μL].

Cytosense was configured to randomly take a maximum of 300 pictures per sample. Each photo represented an individual or a colony such as *Dinobryon* genus. A total of 1000 good-quality photos from the dataset (April and September) were randomly selected, using the *sample_n* function of the *dplyr* package of the R 3.16 software, and subsequently analyzed. The organisms on the photos were manually measured using the *ImageJ 1.53e* software. The length and width of each organism were used for the calculation of the cell biovolume. Then, the biovolume data were used to create a biovolume prediction model with the *RandomForest* package of the R 3.16 software. The coefficient of determination of the linear regression analysis between the manually calculated biovolume and the predicted biovolume was 0.72. The details of the method are presented in the Supplementary Information section (Method S1).

Monitoring data

Meteorological data are available from Le Bouveret, the harbor next to the Rhône River mouth (MeteoSwiss, https://gate.meteoswiss.ch/idaweb); Rhône River discharge, temperature, turbidity and water quality data were measured at the Porte du Scex (Swiss Federal Office of the Environment, OFEV, https://www.hydrodaten.admin.ch/fr/2009.html), and vertical profiles of physico-chemical parameters were

measured at the monitoring station SHL2 on the 1 April and the 24 September (CIPEL/INRA, Rimet 2020).

Calculations

Mixing proportions

The presence of Rhône River water in the lake and the corresponding proportions of Rhône and lake waters mixed at the selected sampling location were quantified from the following isotope mass balance equation (Halder et al. 2013):

$$\delta^{18}O_R x_R + \delta^{18}O_L x_L = \delta^{18}O_S \tag{1}$$

where $\delta^{18}O_R$ is the isotopic composition of the Rhône River water. This parameter is measured once a month proportionally to the discharge by the Swiss Federal Office of the Environment at the Porte du Scex station. It was also measured from our ISCO samples to evaluate the daily fluctuations during the campaigns (Figure S4). For the September campaign, $\delta^{18}O_R$ was calculated as the average of the measurements of the corresponding sampling day that showed a standard deviation close to the analytic error. However, for the April campaign showing important variations of the Rhône signal, the $\delta^{18}O_R$ was selected regarding the sampling time and the closest Rhône sample. $\delta^{18}O_S$ is the isotopic composition of the water measured at the sampling location. The uncertainty of the Rhône River fraction related to the analytic error of $\delta^{18}O_S$ ($\pm 0.05‰$) is evaluated as $\pm 2\%$. $\delta^{18}O_L$ is the value of the mixed, unstratified lake water column that is, for example, homogeneous over the whole lake after a complete overturn. This value is constant at -12.1 ‰ for $\delta^{18}O$. x_L is the mole fraction of lake water at the sampling location. Assuming that there is no other significant contribution in the studied parts of the lake, it was assumed that $x_R + x_L = 1$. Hence, the mole fraction of Rhône water at the sampling location was calculated from:

$$x_R = \frac{(\delta^{18}O_S - \delta^{18}O_L)}{(\delta^{18}O_R - \delta^{18}O_L)} \tag{2}$$

Water column stability

The software Lake Analyser (Read et al. 2011) was used to estimate the stratification strength as measured by the squared Brunt–Väisälä frequency:

$$N^2 = \frac{g}{\rho} \frac{\delta\rho}{\delta z} \tag{3}$$

where g is the acceleration due to gravity, ρ is the water density calculated according to the combined effects of salinity and water temperature based on the equation of

Millero and Poisson (1981), and $\delta\rho/\delta z$ is the density depth gradient calculated by the slope for each meter of the water column. Additionally, the thermocline depth and the thickness of the metalimnion for the temperature profiles of the September campaign showing a clear stratification, contrary to the April campaign's profiles, were calculated.

Grouping and statistical analysis

To determine the impact of the Rhône water intrusion on the nutrient composition and primary production of the surrounding lake water, groups of sampling points in different lake zones were defined. In April, three groups relative to the Rhône water fraction were defined (Figure S5):

- An ambient (lake) zone, outside of the river plume, defined by the absence of Rhône River water (less than 2%, the uncertainty of the Rhône River water fraction)
- An intermediate zone between the Rhône interflow and the ambient zone with a Rhône River water fraction between 2 and 10%
- A core zone of the Rhône interflow with Rhône River water fraction higher than 10%

In September, three groups were defined relative to the Rhône water fraction and the detection of Rhône interflow current velocity, i.e. velocity higher than the typical background current in the lake of 10 cm/s (Figure S6):

- An ambient (lake) zone, with neither Rhône interflow current velocity nor Rhône water (v−/w−)
- A zone without Rhône interflow current velocity but with Rhône water (v−/w+)
- A zone with both Rhône velocity and water detected (v+/w+)

An ANOVA was performed (using the function *anova1* of MATLAB 2021b) to detect significant differences between the groups, revealing a nutrient input or a dilution effect by the river into the lake. To describe the data and detect potential river-induced nutrient contributions to the river–lake transition zone, linear regression analyses were applied to the data according to their distribution (using the linear modelling method *lm* of the *geom_smooth* function of R 3.16). The fraction of Rhône water was used as an explanatory variable and the nutrient concentrations as response variables. Regression diagnostic tests were used to evaluate the strength of such regression (using the function *plot* of R 3.16, Figure S7). According to the data distribution and the regression diagnostic tests, linear regression analyses were applied for descriptive purposes to the silicate data for both seasons and to the orthophosphate data for September. The

statistical analyses were performed with a significance level of $\alpha = 0.05$.

Results

Meteorological, river and lake conditions during the sampling campaigns

April conditions

The weather conditions were quite different between the two sampling days in April (Figure S8). The atmospheric temperature strongly decreased between 2 April (median values of 10.5 °C) and 4 April (2 °C). Wind conditions were calm during the sampling days but a short period of strong wind was noted between them. On the 3 April, a north-westerly wind blew for several hours reaching 14 m/s leading to surface lake currents in excess of 20 cm/s (Figure S9). Consequently, calculations of water column density at stations A-Ib and A-1/I indicated a wind-induced mixing of the water column down to 35 m depth coupled with the advection of open lake water to the Rhône River mouth (Figure S10).

Because of a cold front passing through, linked with high rainfall amounts, the Rhône River temperature decreased between the 2 and the 4 April, from 7.4 to 5.2 °C (median values, Figure S11). The discharge changed from 125 to 205 m³/s and the conductivity decreased from 355 to 295 µS/cm.

On 1 April, the lake had a weak spring thermal stratification with surface water reaching 10 °C (deep water background value of 5.8 °C, Figure S12). No surface mixed layer was detected but a shallow thermocline at 2.5 m depth was already established. The concentration of orthophosphates was low in the upper 30 m with an average of 3 µg P/L. Monitoring profiles taken during the previous winter (Figure S13) showed that only a partial overturn of the lake water occurred, with the lake mixing down to 135 m, compared to the full depth of 309 m (CIPEL 2020). This limits the input of orthophosphates from the deep waters to the euphotic zone. During this period, the phytoplankton community was dominated by diatom species like *Asterionella formosa* and *Ulnaria delicatissima var. angustissima*.

September conditions

The weather conditions were quite similar between the two sampling days in September (Figure S14). The wind speed slightly decreased between the two sampling days with median values of 2 and 1.5 m s⁻¹ on the 24 and the 26 September, respectively.

The river discharge was relatively constant from the 24 to the 26 September with median values of 195 and 197 m³/s,

respectively (Figure S15). During the two sampling days, the river temperature median values were between 8 and 9 °C, which is lower than the lake surface mixed layer temperature measured at SHL2 (see below).

The lake was stratified at that time of the year (Figure S16). The temperature was 17.8 °C in the surface mixed layer and decreased below 7 m to 5.9 °C in the hypolimnion. The concentrations of orthophosphates and silicate in the upper 30 m were lower than in April with an average of 1 µg P/L and 0.38 mg/L, respectively. A peak of turbidity (2.3 FTU) was located around 14 m depth. It correlated with a high concentration of particulate organic carbon, nitrogen and phosphorus. Biological observations showed that this peak corresponded to *Planktothrix rubescens*, a filamentous cyanobacterium.

Rhône River tracing

In April, no significant difference from the reference isotope composition of the lake water was detected at the three stations sampled in the *Grand Lac* (stations A-2, A-3 and A-4, Figure S17a). Meanwhile, a substantial interflow of Rhône River water was detected in the *Haut Lac* between 3 and 30 m depth both in terms of the stable isotope composition of water, conductivity and turbidity (profile A-1, Fig. 3). The next sampling day, after the strong north-west wind event, the interflow disappeared from the 3–30 m depth layer and was detected between 55 and 80 m depth at the same station (profile A–I, Fig. 3). At the station A-II, halfway to the river mouth, no significant isotope anomaly was measured (Figure S18a) but a turbidity signal was measured at the bottom of the Rhône canyon (Figure S19c). No interflow water of the Rhône was detected at the western station A-IV while turbid Rhône water was measured in the eastern shallow area of station A-III (Figure S18a, b). Finally, at the location called *La Bataillère* (station A-V), turbid and cold Rhône water was observed floating on the lake water (Figure S18a, b).

In September, Rhône River discharge was detected in the interflow all along the transversal transect T1-S between 20 and 30 m depth in terms of the stable isotope composition, turbidity and a negative conductivity anomaly marked by a river-induced dilution of lake water (Figs. 4 and S18b, c). The Rhône interflow was centered at 20 m depth below the averaged thermocline depth detected at 15 m in the temperature profiles of transect T1-S (Table S3). In terms of the normal component of velocities, the interflow was only detected at stations S-I, S-III and S-IV. On the river-to-open-lake transect T2-S, the Rhône interflow was concentrated at around 30% in its core zone in the near field area (stations S-1 to S-3) and around 20% outside (stations S-4 and S-5, Fig. 5). The core zone was located at about 25 m depth, still below the thermocline detected at about 19 m depth (Table S3). Due to an increase in Rhône conductivity during
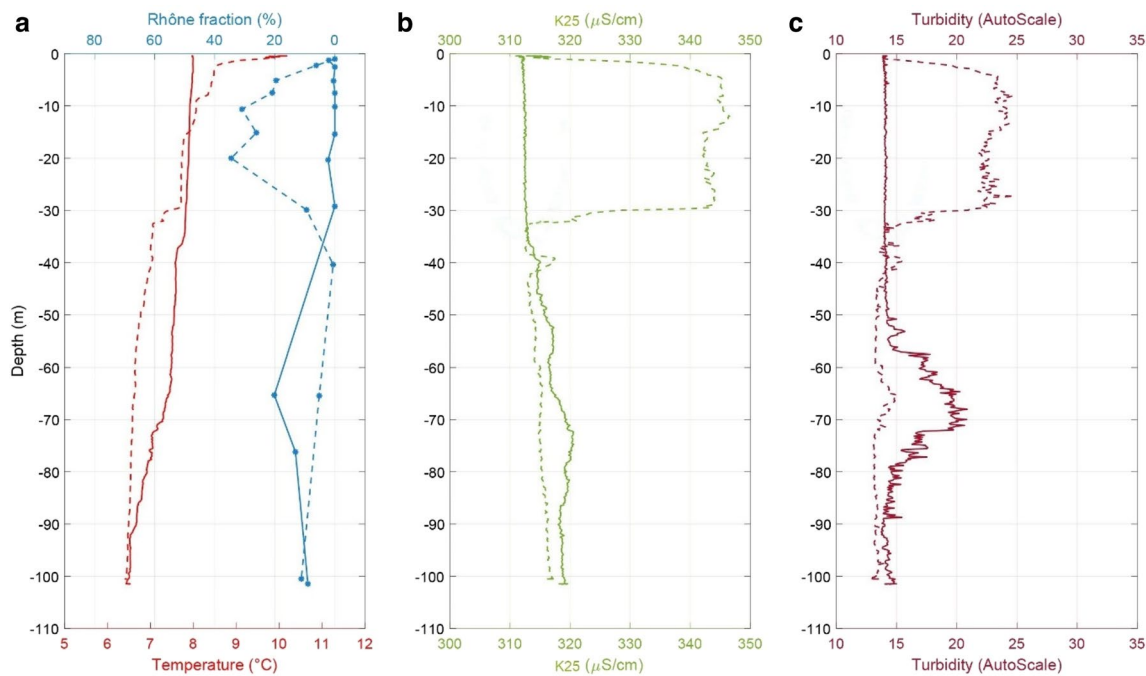
Fig. 3 Water column mixing to 35 m depth by the wind event of the 3 April. Vertical profiles of Rhône fraction in blue and temperature in red (**a**), conductivity K25 (**b**) and turbidity (**c**) at station A-1/I. Profile A-1 (before the wind event, the 2 April) shown as a dashed line and profile A-I (after the wind event, the 4 April) as a continuous line
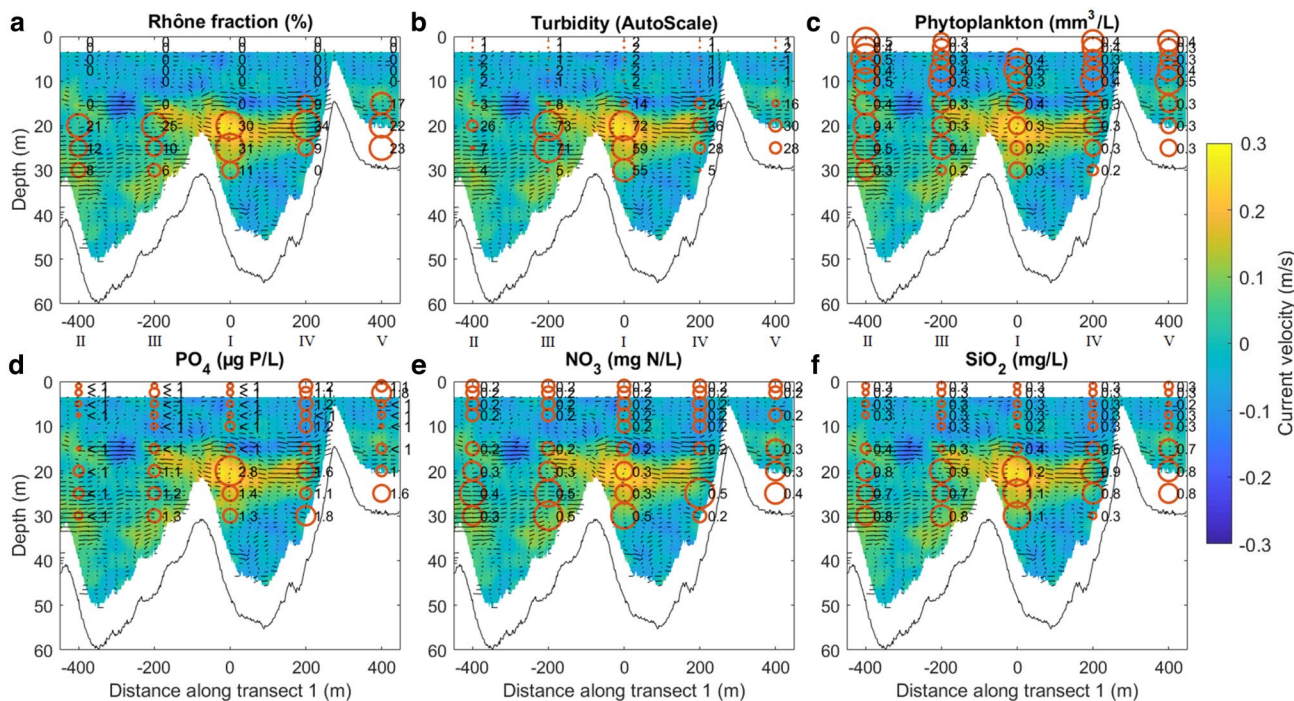

Fig. 4 Vertical profiles of Rhône fraction (**a**), turbidity (**b**), phytoplankton biovolume (**c**), orthophosphates (**d**), nitrate (**e**) and silicate (**f**) at the stations of transect T1-S (from left to right: II–III–I–IV–V) with parameter values indicated by red circles and the normal component of the velocity current indicated by the background colormap (value) and the arrows (direction). The position 0 along transect 1 corresponds to central station I in front of the river mouth. The black line at the bottom indicates the lakebed
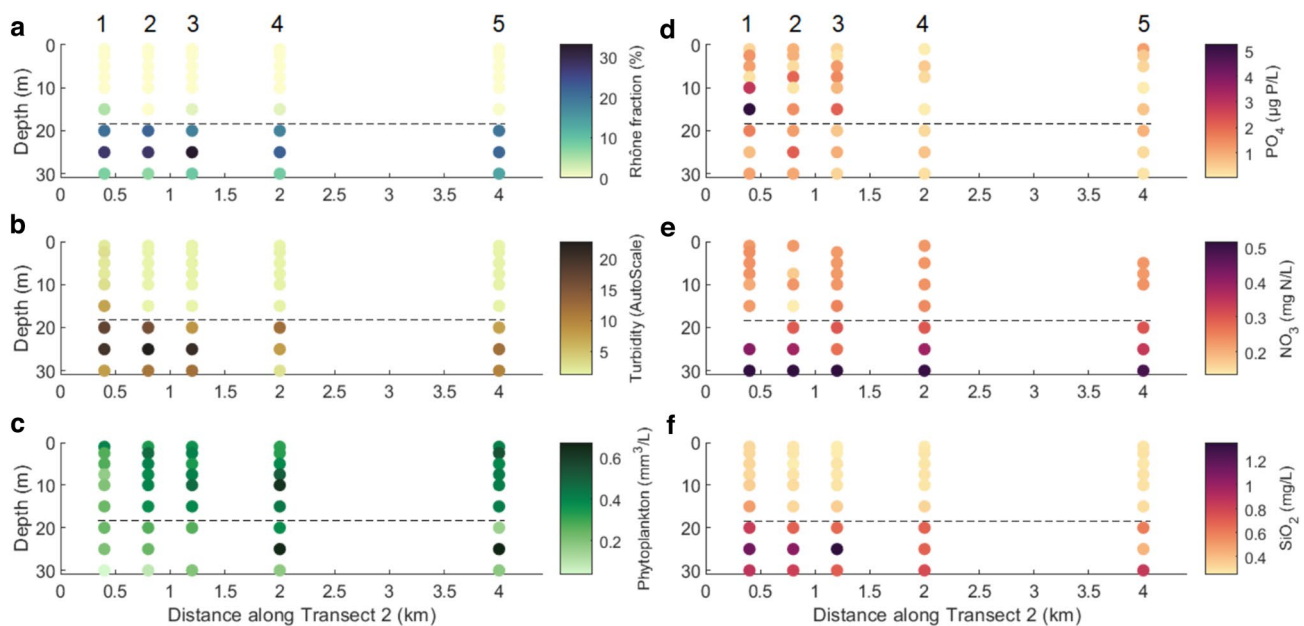
Fig. 5 Vertical profiles of Rhône fraction (**a**), turbidity (**b**), phytoplankton biovolume (**c**), orthophosphates (**d**), nitrate (**e**) and silicate (**f**) at the stations of transect T2-S (from left to right: 1–2–3–4–5). The position 0 along transect 2 corresponds to the river mouth. The dashed line represents the average depth of the thermocline. The limit of the near field was detected at station 4 by ADCP profiling (see Figure S3)

26 September, the interflow conductivity anomaly was less marked (Figure S20b). In terms of turbidity, the intrusion was still well detectable. Moreover, turbidity was measured at the bottom of the canyon at stations S-1 to S-4, along with lower $\delta^{18}O$ values (Figure S20c).

Nutrient concentrations

There is a net input of orthophosphates from the river to the lake during the two seasons (Fig. 6). Even with a notable variation of phosphate concentrations within the Rhône River, there are significant differences between the river, the core and the intermediate zone concentrations (ANOVA tests in Table 1). It is important to note that the background concentration of phosphorous in the lake was already low in April and was at the same level during September (around 1 µg P/L), whereas the Rhône concentration was on average twice as high in spring compared to early fall (7.6 vs 3.6 µg P/L). The linear regression analysis applied to the orthophosphate data of September showed a positive trend related to the Rhône River fraction indicating a phosphate contribution of the Rhône to the river–lake transition zone ($R^2 = 0.38$ and p value < 0.001, Fig. 7b).

In April, no significant input or dilution effect was noted for the nitrate concentrations (Fig. 6a). In September, the nitrate concentration was higher in the Rhône (0.32 mg N/L) compared to that in the lake (0.22 mg N/L). However, by looking at the depth profiles (Fig. 5e), such higher concentrations in the interflow are mainly due to the depth gradient of nitrate in the lake.

The silica concentration also showed an important depth gradient with an increase in depth at the beginning of autumn due to the biological uptake by diatom species all along the growing season in the surface layers (CIPEL 2020). The river input of silica was, however, higher than the silica concentration of the ambient lake at the interflow depth. This correlates so with the Rhône River fraction and leads to a significant river contribution in silica to the transition zone ($R^2 = 0.90$ and p value < 0.001, Fig. 7b), as was noted in April ($R^2 = 0.62$ and p value < 0.001, Fig. 7a). In transect T2-S, the river intrusion in the water column is evident from the isotopic composition of water and the silica concentration. Both diminish with distance from the river mouth and with consequent mixing with ambient lake water (Fig. 5a, f).

Phytoplankton biovolume

Phytoplankton biovolumes were significantly different between the groups (ANOVA tests in Table 1) and showed the same pattern for the two seasons: the core zone of the interflow with the strongest current and the highest turbidity had the lowest biovolume, followed by the intermediate zone and the ambient zone (Fig. 6). There was, however, a difference in scale: in April the algal biovolume was almost three
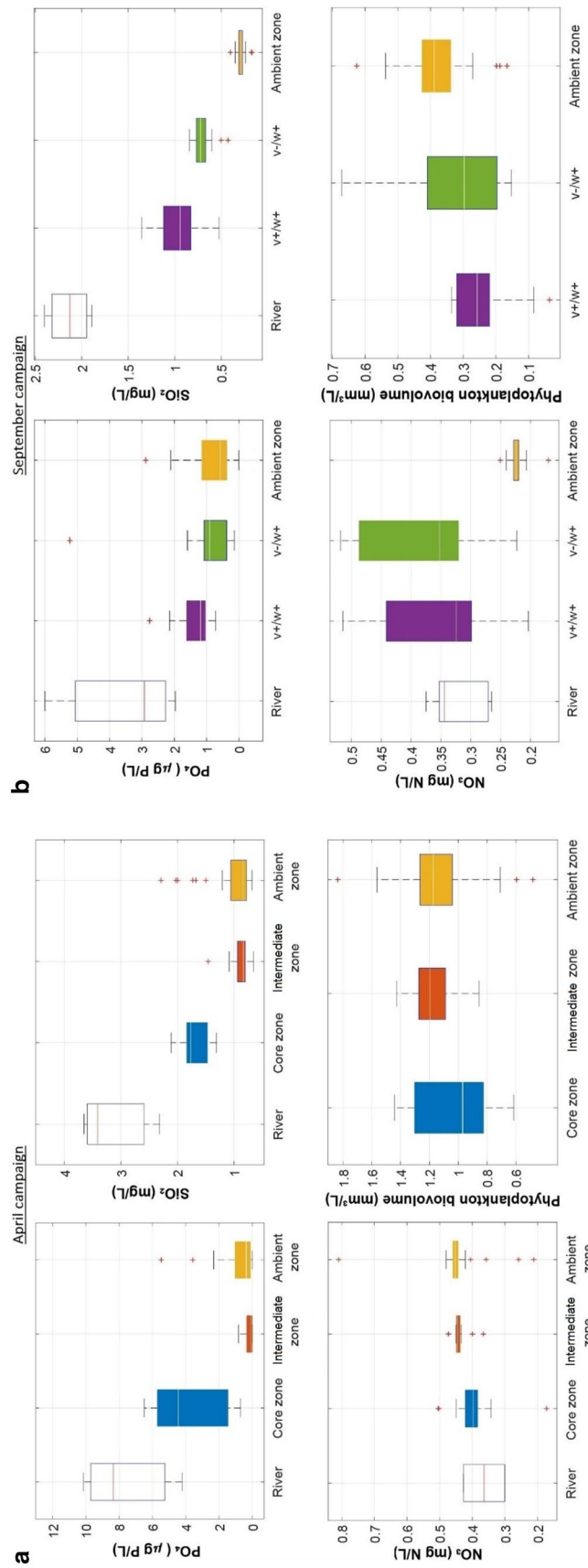
Fig. 6 Boxplots of concentrations relative to April groups (**a**) with $n_{River} = 3$, $n_{Core\ zone} = 14$, $n_{Intermediate\ zone} = 13$, $n_{Ambient\ zone} = 55$. For both seasons, the 'Ambient zone' represents a zone of the lake without Rhône intrusion trace. In April, the 'Core zone' represents a zone with a Rhône water fraction higher than 10% and the 'Intermediate zone', a zone with a Rhône water fraction between 2 and 10%. In September, the 'v+/w+' group represents a zone with both Rhône interflow current velocity and Rhône water detected and the 'v−/w+' group, a zone without Rhône velocity but with Rhône water. For each box, the central mark indicates the median, and the bottom and top edges of the box indicate the 25th and 75th percentiles, respectively. The whiskers extend to the most extreme data points not considered outliers, and the outliers are plotted individually using red crosses. The ANOVA tests point out significant differences between the groups (p values <0.05) for all the parameters except for NO_3^- in April (Table 1)

Table 1 Results of ANOVA tests (function *anova1* of MATLAB) with the different groups of the April campaign (a) and September campaign (b)

	Source	SS	df	MS	F	p value
(a) April campaign						
	Groups	229.574	3	76.5246	43.4	7.10×10^{-16}
PO_4^{3-}	Error	121.655	69	1.7631		
	Total	351.229	72			
	Groups	0.03686	3	0.01229	2.32	0.084
NO_3^-	Error	0.33901	64	0.0053		
	Total	0.37587	67			
	Groups	17.3437	3	5.78125	46.85	1.01×10^{-16}
SiO_2	Error	8.6387	70	0.12341		
	Total	25.9824	73			
	Groups	2.05×10^7	2	1.02×10^7	8.57	5×10^{-4}
Phytoplankton	Error	7.16×10^7	60	1.19×10^6		
	Total	9.21×10^7	62			
(b) September campaign						
	Groups	38.9617	3	12.9872	19.6	8.55×10^{-10}
PO_4^{3-}	Error	57.6574	87	0.6627		
	Total	96.6192	90			
	Groups	0.42341	3	0.14114	39.44	2.91×10^{-15}
NO_3^-	Error	0.26123	73	0.00358		
	Total	0.68464	76			
	Groups	19.0111	3	6.33705	517.81	2.41×10^{-55}
SiO_2	Error	1.0647	87	0.01224		
	Total	20.0759	90			
	Groups	412,648.3	2	206,324.2	5.02	0.009
Phytoplankton	Error	3,287,468.6	80	41,093.4		
	Total	3,700,116.9	82			

SS is the sum of squares due to each source. df is the degree of freedom associated with each source. MS is the mean square for each source, which is the ratio SS/df. F statistic is the ratio of the mean squares. The p value is the probability that the F statistic can take a value larger than the computed test-statistic value

times higher than in September, with respective averages of 1.15 mm³/L vs 0.39 mm³/L in the ambient zone.

Concerning the biovolume of phytoplankton relative to the distance from the Rhône inflow, the minimum was located close to the river mouth, at station A-1, on 2 April, with a profile average of 0.86 mm³/L. A maximum of 1.22 mm³/L was measured at station A-2, 5 km from the river mouth, and a lower value of 1.04 mm³/L in the middle of the lake (station A-4, Fig. 8a). On 4 April, after the wind-induced mixing of the water column down to 35 m depth, the profile's average of phytoplankton biovolume increased by 44% at station A-1/I. Moreover, it seems to be homogenized in the *Haut Lac* with concentrations averaging 1.22 mm³/L at stations A-I, A-III and A-IV with a vertical standard deviation that decreased at station A-I. Meanwhile, the values at station A-V, just in front of the Rhône, stayed low with an average of 1.13 mm³/L.

On 24 September, the phytoplankton distribution was vertically heterogeneous in front of the river mouth (T1-S, Fig. 4) with low values below the thermocline and slightly more elevated in the epilimnion, averaging 0.31 and 0.39 mm³/L, respectively. Horizontally, the phytoplankton biovolumes were higher at station S-II with an average of 0.44 mm³/L compared to the other stations of T1-S with an average of 0.34 mm³/L (Fig. 8b). The vertical profile at station S-II also showed the less intense turbidity plume on transect T1-S (Fig. 4). On 26 September, the biovolumes decreased at all depths of station S-I/1. Biovolumes were especially low at station S-1 in front of the Rhône with an average of 0.22 mm³/L. Then, it increased progressively with the distance from the river mouth to reach an average of 0.40 mm³/L at station S-5 located at 4 km (Fig. 8b). At 25 m depth, at the depth of the core zone of the interflow, the biovolumes were relatively low in the near field (stations S-1 and S-2) with an average of 0.22 mm³/L, but then increased by a factor of 3 outwards with maxima of 0.66 and 0.67 mm³/L at stations S-4 and S-5, respectively (Fig. 5). These maxima were also 64% higher than the averaged biovolume between 0 and 20 m depth at the same stations.
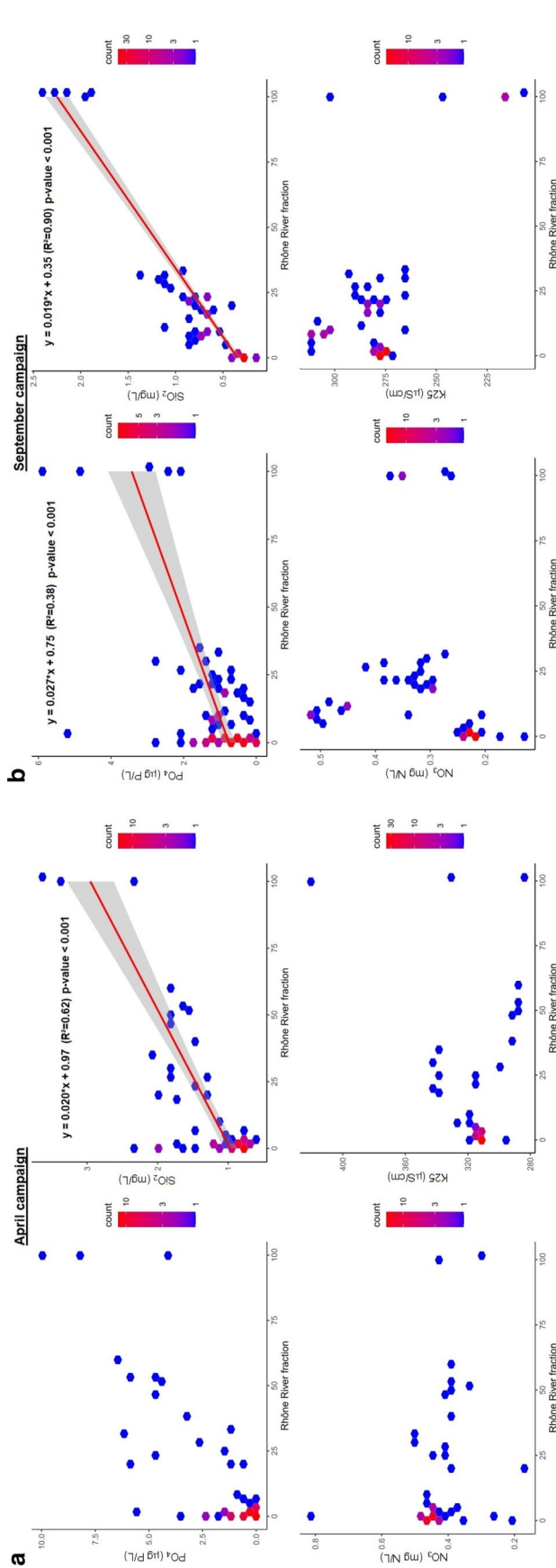
Fig. 7 Hexbin plot of nutrient concentrations and conductivity K25 relative to the Rhône River fraction for the April campaign (**a**) and September campaign (**b**). The color of each hexagon denotes the frequency of data points in it. Linear regression analyses were applied for descriptive purposes to the silicate data for both seasons and to the orthophosphate data for September (see diagnostic tests in Figure S7). The linear regression (linear modelling method *lm* of the *geom_smooth* function of R 3.16) is bounded by the 95% confidence intervals. Reported are the equation of the linear model, the coefficient of determination (R^2) and the significance level (*p* value)

Fig. 8 Boxplots of phytoplankton biovolume relative to April stations (**a**) of T2-A (4 to 1) and T1-A (I, III, IV and V) and relative to September stations (**b**) of T1-S (I to V) and T2-S (1 to 5). For each box, the central mark indicates the median, and the bottom and top edges of the box indicate the 25th and 75th percentiles, respectively. The whiskers extend to the most extreme data points not considered outliers, and the outliers are plotted individually using red crosses. The ANOVA tests point out significant differences between the phytoplankton biovolume profiles of each station with *p* values < 0.05 for both seasons (Table S4)
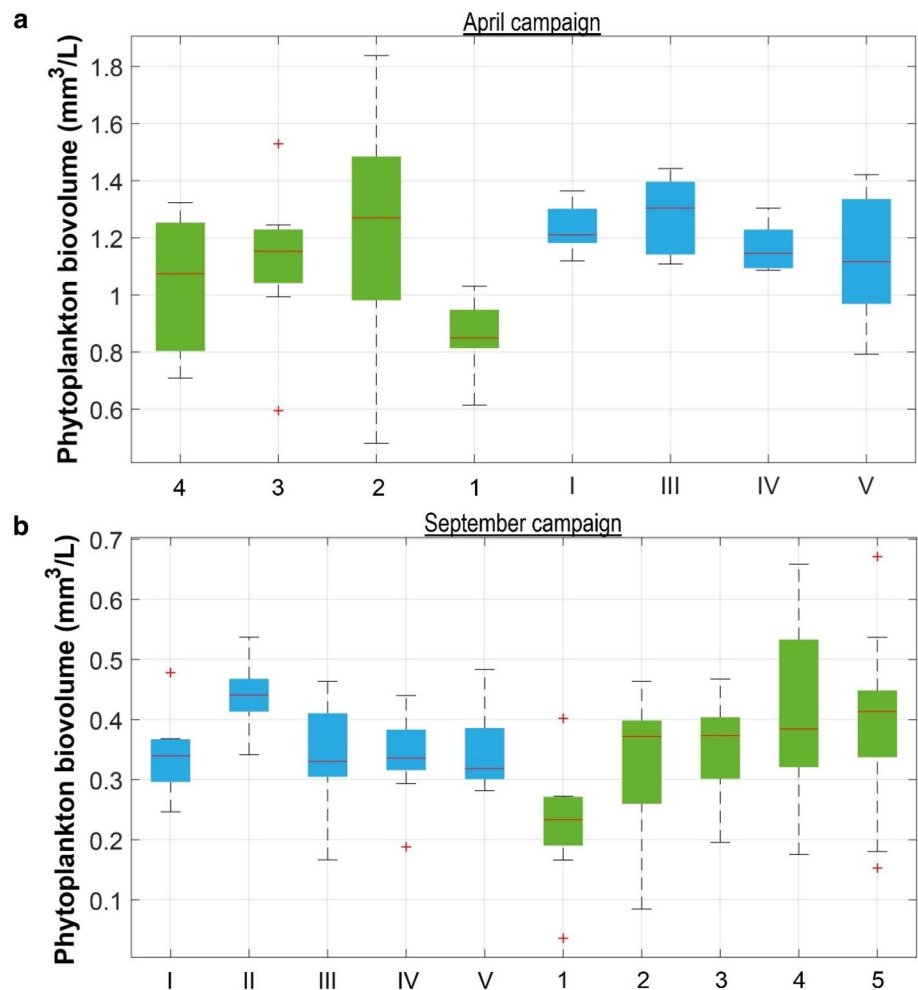
Discussion

Rhône River intrusion

The conductivity of the Rhône River varies as a function of its seasonally different hydrological conditions. In spring and summer, when the Rhône River is mainly fed by snow and glacial melt waters, the dissolved major ions transported by the Rhône (80% of carbonate ions, sulphate ions and associated calcium) are diluted by the higher discharge. Often short-term changes in major ion concentrations can be caused by the operation of dams for the generation of hydropower in the catchment of the upper Rhône. Consequently, a positive or a negative anomaly in conductivity can be detected in the lake at the location of the Rhône River interflow within one week or even a single day, as noted during the April campaign. In September, the conductivity of the Rhône was measured to be lower than that of the lake (230 compared to 260–300 µS/cm), thus resulting in a negative anomaly at the interflow depth. Therefore, conductivity alone and its relative change cannot be used to detect the

Rhône water interflow or to identify a chemical gradient related to the interflow only. Nevertheless, significant river inputs of orthophosphates and silica were measured within the river–lake transition zone (Figs. 6 and 7).

In terms of turbidity, the Rhône River plume was detectable in and out of the near field area. The turbidity signal corresponds to the presence of the interflow, likely supported by higher flow velocities within the interflow close to the river mouth, as seen in the transversal transect (T1-S, Fig. 4). The turbidity had maximum values in the near field but decreased with distance out of this zone (T2-S, Fig. 5). However, a turbidity anomaly could still be measured at the background station S-5. As noted already by Giovanoli (1990) and Escoffier et al. (2022), the fine fraction of the sediments as well as likely additional authigenic minerals can stay in suspension within the Rhône River interflow.

Moreover, the turbidity measured at the bottom of the canyon at stations S-1 to S-4 (Figure S20c), along with lower δ^{18}O values, suggests a stacking of an interflow and an underflow. This may represent two different periods of Rhône River injection with different densities, or perhaps a

splitting of the river inflow into two: an interflow concentrated in river water that intrudes into the thermocline and a gravity current that follows the bottom of the canyon (Cortés et al. 2014b). However, this presence of Rhône water in the deeper part of the lake did not generate any nutrient gradient as the measured Rhône fractions represent a small proportion (≤6%), and the nutrient concentrations of the ambient lake at these depths are either close to those of the Rhône (Si) or, in the case of P and N, higher (Table S2).

Furthermore, some vertical profiles in the near field (at stations S-II and S-V in T1-S, Fig. 4) indicated the presence of Rhône River water even where no changes in velocity were measurable. This can be explained by the variable hydrodynamics within this area. Depending on the discharge of the river, its density and the lake currents, the interflow can establish itself at a restricted depth close to the entry point, but subsequently change its location as these parameters fluctuate on relatively short time scales (Soulignac et al. 2021). Out of the near field area (stations S-4 and S-5 of T2-S, Fig. 5), the river momentum is insufficient to control the interflow dispersion. The interflow, stabilized in a specific layer within the metalimnion due to its buoyancy, is then transported by the lake currents (Cimatoribus et al. 2019; Cotte and Vennemann 2020).

Previous studies demonstrated the capacity of the stable isotope composition of water to trace the Rhône River interflow within the entire lake (Halder et al. 2013; Cotte and Vennemann 2020). In the present study, no trace of the Rhône interflow water was detected for the measured vertical profiles outside of the river mouth area in April. The condition for the interflow to reach further into the lake, i.e., a strong stratification, was not yet established. Consequently, the Rhône River nutrients stayed in the *Haut Lac* and were preferentially bioavailable in the euphotic zone of this part of the lake when wind events occurred during this season (see below). Alternatively, the Rhône River may intrude deeper into the hypolimnion when the thermal stratification is weakened as seen after the wind event in April or during the winter season (Cotte 2021).

The river–lake transition zone: a dynamic area

Some hydrodynamic processes capable of changing the Rhône River intrusion pattern were detected. These can potentially change the nutrient and biological gradients and make the river–lake transition zone highly dynamic.

First, the wind event of 3 April broke the early stratification and mixed the water column to 35 m depth with advected open lake water (Figs. 3 and S9). It was noted with the measurement on 4 April that the Rhône signal in terms of isotope composition, turbidity and nutrient concentration disappeared from the top 30 m (Figure S17). In addition, the newly established density gradient and thermocline,

which briefly established itself at 70 m depth, and the colder atmospheric and river temperatures (Figures S8, S10 and S11) forced the Rhône to intrude into the water column well below the euphotic zone. However, at this depth, no significant Rhône nutrient input was detected because the nutrient concentrations in these layers of the lake already correspond to those of the Rhône. This event illustrates the impact of the quickly changing meteorological and hydrological conditions on the river intrusion pattern.

Then, the river intrusion depth can change rapidly even during a period of strong stratification. Indeed, in September, despite a lower density on the 26th compared to the 24th (higher temperature and lower sediment load, Figure S15), the Rhône intruded 5 m deeper, following the deepening of the thermocline occurring in between the two sampling days. Consequently, this deepening of the intrusion led to a deepening of the river nutrient input with a maximum of silica concentration first, measured at 20 m depth, then at 25 m depth (Figs. 4 and 5). With relatively homogenous meteorological conditions during these two days (Figure S14), these results show how the depth of the river intrusion and its nutrients can be influenced by the lake stratification (Cotte and Vennemann 2020; Soulignac et al. 2021).

A dynamic ecocline in the river–lake transition zone

The nutrient contributions observed in the river–lake transition zone are strongly impacted by the hydrodynamic processes described above. In addition, the displacement of the Rhône River turbidity plume makes the conditions for phytoplankton growth highly variable.

Indeed, during April, the early thermal stratification allowed the Rhône nutrients to be transported as an interflow into the shallow metalimnion. However, the presence of an opaque turbidity plume in the river mouth area related to the Rhône water intrusion (profile A-1, Fig. 3) seemed to block the sunlight penetration and inhibit the phytoplankton development. After the wind-induced mixing of the water column and the deepening of the Rhône intrusion, the turbidity dropped in the top 30 m, allowing the phytoplankton biovolume to expand by 44% (averages of profile A-I compared to profile A-1, Fig. 8a), while it stayed relatively low in the turbid plunge zone (station A-V). In September, a significant input of P and Si was measured, but no fertilization effect was observed in the river mouth near field (T1-S, Fig. 4). Similarly, the phytoplankton development seemed to be limited by the sediment plume of the Rhône interflow and its important current velocity as illustrated by the difference of phytoplankton biovolumes between the groups with and without Rhône interflow current velocity (on average 0.24 vs 0.33 mm^3/L, respectively, Fig. 6). Instead, out of this turbid near field, at the Rhône intrusion depth, there was a strong increase of phytoplankton biovolume by a factor of 3 (T2-S, Fig. 5). River intrusions occurring in

the metalimnion can fuel algal growth and lead to the development of a deep chlorophyll maximum (Cortés et al. 2014a, b). Here, we observed this phenomenon but only outside of the hydrodynamically-defined near field of the river mouth.

Using remote sensing, Kiefer et al. (2015) and Soomets et al. (2019) measured, respectively, a higher Chl *a* concentration and a higher primary production in the eastern part of Lake Geneva and hypothesized a relationship with the proximity of the Rhône input. Moreover, Kiefer et al. (2015) measured the highest variability of Chl *a* in this area around the Rhône inflow, especially in spring. Our results suggest that these observations can be explained by the highly variable Rhône River intrusion pattern. During our study, we saw that the turbidity plume induced by the Rhône interflow may limit phytoplankton growth at greater depth in the near field area. Then, if the river intrusion depth changes or we move out of this near field, phytoplankton development can be enhanced. This was shown here through the increase of phytoplankton biovolume in the euphotic zone following the wind-induced deepening of the river intrusion in April and by the deep chlorophyll maxima observed in September. Finally, our results reveal that an ecocline can develop in the transition zone between the Rhône River and Lake Geneva where equilibrium occurs between the river limiting factors (temperature, light and low flow velocities) and those that are limiting phytoplankton development in the lake (nutrient concentrations, P and Si). However, these optimal conditions are temporally and spatially dynamic depending on the river intrusion pattern, itself determined by the meteorological, hydrological and lake conditions.

Using satellite images and a hydrodynamic model, Soulignac et al. (2018) indicated an earlier onset of phytoplankton development in spring 2011 in the *Haut Lac* compared to the rest of the lake. They argued that this sheltered area may favor an earlier stratification and hence improved access to light, leading to an earlier onset of the spring bloom. We can add that the Rhône River nutrients start to intrude in the metalimnion in this part of the lake at the beginning of spring. Then, as observed, a subsequent wind event can disrupt the weak stratification, homogenize the euphotic zone where the Rhône intruded and limit further transport of its nutrients. As a consequence, the Rhône nutrients stay in the *Haut Lac* and this eastern part of the lake (station A-I), except for the turbid near field area (stations A-1 and A-V), presents optimal conditions for the phytoplankton growth in contrast to the central lake (station A-4).

Summary and conclusions

Significant contributions of P and Si were measured in this transition zone related to the Rhône River intrusion. However, this nutrient input did not necessarily induce a fertilization effect because of the inhibition of the phytoplankton growth by the Rhône sediment plume.

Additionally, the river–lake transition zone was identified as a dynamic area. Indeed, the varying patterns of the Rhône River intrusion related to the meteorological and hydrological conditions, as well as the lake stratification, changed the characteristics of the observed ecocline. In early spring, the thermal stratification was too weak to allow the Rhône River interflow to reach the central part of the lake. Despite a net input of phosphorus, the phytoplankton growth was limited by the turbid Rhône River plume close to the river mouth. However, a sudden cooling and wind event forced the Rhône River to intrude deeper, reducing the turbidity within the euphotic zone and leading to an increase of 44% in the phytoplankton biovolume. Then, the deep intrusion of river nutrients in September seems to maintain an autumnal phytoplankton development when the euphotic layer is depleted in nutrients. This fertilization effect was measured at the Rhône interflow depth beyond where the sediment plume inhibited the phytoplankton growth. Therefore, this study showed that the river–lake transition zone between the Rhône River and Lake Geneva, except its turbid near field, is a dynamic area where local optimal conditions can promote phytoplankton growth contrary to the central depleted basin.

Consequently, these results suggest that the existing two monitoring stations may not be sufficient to understand the phytoplankton dynamics of the lake. To do so, as argued by Kiefer et al. (2015), the river–lake transition zones have to be taken into account. This study confirms that the influence of the Rhône River intrusion on primary production should be considered to fully understand the phytoplankton distribution within the lake.

Moreover, complete lake overturns in winter are expected to occur less frequently in the future due to climate change (Perroud et al. 2009). As measured during winter 2019, partial mixing of the water column limited the upward input of nutrient-richer water. In this context, the Rhône River interflow and its related nutrients supply to the euphotic zone is expected to have a more notable impact on the primary production of the lake. Hence, the river–lake transition zone between the Rhône River and Lake Geneva should gain in attention. Then, the temporal resolution should be improved for future comprehensive studies of such dynamic ecosystems. For example, an in-depth study of the extent of the Rhône-induced nutrient gradients and the related fertilization effect in the lake could be done by using the scientific platform LéXPLORE (Wüest et al. 2021). This platform, located 20 km northwestward of the Rhône River mouth, allows a high temporal density monitoring of the water column. Finally, such poorly documented process of wind-induced mixing of the water column and its impact on the phytoplankton distribution in a river–lake transition zone, their frequency and their impact on the whole lake

ecosystem dynamic could be studied by coupling remote sensing, 3D numerical modeling and point-wise field measurements.

Declarations

Conflict of interest The authors have no competing interests to declare that are relevant to the content of this article.

References

Anneville O, Beniston M, Gallina N, Gillet C, Jacquet S, Lazzarotto J (2013) L'empreinte du changement climatique sur le Léman. Arch Sci 66:157–172

Anneville O, Dur G, Rimet F, Souissi S (2018) Plasticity in phytoplankton annual periodicity: an adaptation to long-term environmental changes. Hydrobiologia 824:121–141. https://doi.org/10.1007/s10750-017-3412-z

Attrill MJ, Rundle SD (2002) Ecotone or ecocline: ecological boundaries in estuaries. Estuar Coast Shelf Sci 55:929–936. https://doi.org/10.1006/ecss.2002.1036

Baracchini T, Wüest A, Bouffard D (2020) Meteolakes: an operational online three-dimensional forecasting platform for lake hydrodynamics. Water Res 172:115529. https://doi.org/10.1016/j.watres.2020.115529

Bouffard D, Perga M-E (2016) Are flood-driven turbidity currents hot spots for priming effect in lakes? Biogeosciences 13:3573–3584. https://doi.org/10.5194/bg-13-3573-2016

Carlson Mazur ML et al (2019) Seasonal patterns in hydrochemical mixing in three Great Lakes rivermouth ecosystems. J Great Lakes Res 45:651–663. https://doi.org/10.1016/j.jglr.2019.03.009

Cimatoribus AA, Lemmin U, Barry DA (2019) Tracking Lagrangian transport in Lake Geneva: a 3D numerical modeling investigation. Limnol Oceanogr 64:1252–1269. https://doi.org/10.1002/lno.11111

Conseil scientifique de la commission internationale pour la protection des eaux du Léman contre la pollution (2019) Rapports sur les études et recherches entreprises dans le bassin lémanique. Campagne 2018. CIPEL. https://www.cipel.org/wp-content/uploads/2021/06/rapportscientifique-camp-2018-vf.pdf

Conseil scientifique de la commission internationale pour la protection des eaux du Léman contre la pollution (2020) Rapports sur les études et recherches entreprises dans le bassin lémanique. Campagne 2019. CIPEL. https://www.cipel.org/wp-content/uploads/2021/06/rapportscientifique-camp-2019.pdf

Corella JP et al (2016) The role of mass-transport deposits and turbidites in shaping modern lacustrine deepwater channels. Marine Petrol Geol 77:515–525. https://doi.org/10.1016/j.marpetgeo.2016.07.004

Cortés A, Fleenor WE, Wells MG, de Vicente I, Rueda FJ (2014a) Pathways of river water to the surface layers of stratified reservoirs. Limnol Oceanogr 59:233–250. https://doi.org/10.4319/lo.2014.59.1.0233

Cortés A, Rueda FJ, Wells MG (2014b) Experimental observations of the splitting of a gravity current at a density step in a stratified water body. J Geophys Res Oceans 119:1038–1053. https://doi.org/10.1002/2013JC009304

Cotte G, Vennemann TW (2020) Mixing of Rhône River water in Lake Geneva: Seasonal tracing using stable isotope composition of water. J Great Lakes Res 46:839–849. https://doi.org/10.1016/j.jglr.2020.05.015

Cotte G (2021) Mixing of Rhône River water in Lake Geneva (Léman): implications on the biogeochemistry of the lake. PhD thesis (Chapter II). University of Lausanne. https://serval.unil.ch/en/notice/serval:BIB_A16B0E629D4F

Escoffier N, Perolo P, Lambert T, Rüegg J, Odermatt D, Adatte T, Vennemann TW, Perga M-E (2022) Whiting events in a large peri-alpine lake: evidence of a catchment-scale process. J Geophys Res Biogeosci 127:e2022JG006823. https://doi.org/10.1029/2022JG006823

Ghadouani A, Smith REH (2005) Phytoplankton distribution in Lake Erie as assessed by a new in situ spectrofluorometric technique. J Great Lakes Res 31:154–167. https://doi.org/10.1016/S0380-1330(05)70311-7

Giovanoli F (1990) Horizontal transport and sedimentation by interflows and turbidity currents in Lake Geneva. In: Tilzer MM, Serruya C (eds) Large lakes: ecological structure and function, brock/springer series in contemporary bioscience. Springer, Berlin, Heidelberg, pp 175–195

Halder J, Decrouy L, Vennemann TW (2013) Mixing of Rhône River water in Lake Geneva (Switzerland–France) inferred from stable hydrogen and oxygen isotope profiles. J Hydrol 477:152–164. https://doi.org/10.1016/j.jhydrol.2012.11.026

Jameel Y, Stein S, Grimm E, Roswell C, Wilson AE, Troy C, Höök TO, Bowen GJ (2018) Physicochemical characteristics of a southern Lake Michigan river plume. J Great Lakes Res 44:209–218. https://doi.org/10.1016/j.jglr.2018.01.003

Jenny J-P, Francus P, Normandeau A, Lapointe F, Perga M-E, Ojala A, Schimmelmann A, Zolitschka B (2016) Global spread of hypoxia in freshwater ecosystems during the last three centuries is caused by rising local human pressure. Glob Change Biol 22:1481–1489. https://doi.org/10.1111/gcb.13193

Jenny J-P et al (2020) Scientists' warning to humanity: rapid degradation of the world's large lakes. J Great Lakes Res 46:686–702. https://doi.org/10.1016/j.jglr.2020.05.006

Kiefer I, Odermatt D, Anneville O, Wüest A, Bouffard D (2015) Application of remote sensing for the optimization of in-situ sampling for monitoring of phytoplankton abundance in a large lake. Sci Total Environ 527:493–506. https://doi.org/10.1016/j.scitotenv.2015.05.011

Kremer K, Corella JP, Hilbe M, Marillier F, Dupuy D, Zenhäusern G, Girardclos S (2015) Changes in distal sedimentation regime of the Rhone delta system controlled by subaquatic channels (Lake Geneva, Switzerland/France). Mar Geol 370:125–135. https://doi.org/10.1016/j.margeo.2015.10.013

Larson JH, Trebitz AS, Steinman AD, Wiley MJ, Mazur MC, Pebbles V, Braun HA, Seelbach PW (2013) Great Lakes rivermouth ecosystems: scientific synthesis and management implications. J Gt Lakes Res 39:513–524. https://doi.org/10.1016/j.jglr.2013.06.002

Larson JH, Frost PC, Vallazza JM, Nelson JC, Richardson WB (2016) Do rivermouths alter nutrient and seston delivery to the nearshore? Freshw Biol 61:1935–1949. https://doi.org/10.1111/fwb.12827

Leoni B, Luisa Marti C, Imberger J, Garibaldi L (2014) Summer spatial variations in phytoplankton composition and biomass in surface waters of a warm-temperate, deep, oligoholomictic lake: Lake Iseo, Italy. Inland Waters 4:303–310. https://doi.org/10.5268/IW-4.3.569

Loizeau J-L, Dominik J (2000) Evolution of the upper rhone river discharge and suspended sediment load during the last 80 years and some implications for Lake Geneva. Aquat Sci 62:54–67. https://doi.org/10.1007/s000270050075

Mackay EB, Jones ID, Folkard AM, Thackeray SJ (2011) Transition zones in small lakes: the importance of dilution and biological uptake on lake-wide heterogeneity. Hydrobiologia 678:85–97. https://doi.org/10.1007/s10750-011-0825-y

Makarewicz JC, Lewis TW, Boyer GL, Edwards WJ (2012) The influence of streams on nearshore water chemistry, Lake Ontario. J Great Lakes Res 38:62–71. https://doi.org/10.1016/j.jglr.2012.02.010

Marti CL, Mills R, Imberger J (2011) Pathways of multiple inflows into a stratified reservoir: Thomson Reservoir, Australia. Adv Water Resour 34:551–561. https://doi.org/10.1016/j.advwatres.2011.01.003

Millero FJ, Poisson A (1981) International one-atmosphere equation of state of seawater. Deep-Sea Res 28:625–629. https://doi.org/10.1016/0198-0149(81)90122-9

Moisset S (2017) Investigation of the link between phytoplankton and nutrients dynamic in Lake Geneva. PhD thesis. University of Geneva. https://doi.org/10.13097/archive-ouverte/unige:96830

Morrice JA, Kelly JR, Trebitz AS, Cotter AM, Knuth ML (2004) Temporal dynamics of nutrients (N and P) and hydrology in a lake superior coastal wetland. J Great Lakes Res 30:82–96. https://doi.org/10.1016/S0380-1330(04)70379-2

Murphy J, Riley JP (1962) A modified single solution method for the determination of phosphate in natural waters. Anal Chim Acta 27:31–36. https://doi.org/10.1016/S0003-2670(00)88444-5

Nouchi V, Kutser T, Wüest A, Müller B, Odermatt D, Baracchini T, Bouffard D (2019) Resolving biogeochemical processes in lakes using remote sensing. Aquat Sci 81:27. https://doi.org/10.1007/s00027-019-0626-3

Perroud M, Goyette S, Martynov A, Beniston M, Anneville O (2009) Simulation of multiannual thermal profiles in deep Lake Geneva: a comparison of one-dimensional lake models. Limnol Oceanogr 54:1574–1594. https://doi.org/10.4319/lo.2009.54.5.1574

Read JS, Hamilton DP, Jones ID, Muraoka K, Winslow LA, Kroiss R, Wu CH, Gaiser E (2011) Derivation of lake mixing and stratification indices from high-resolution lake buoy data. Environ Model Softw 26:1325–1336. https://doi.org/10.1016/j.envsoft.2011.05.006

Richardson K, Jørgensen BB (2013) Eutrophication: definition, History and Effects. Eutrophication in coastal marine ecosystems. American Geophysical Union, pp 1–19. https://doi.org/10.1029/CE052p0001

Rimet F et al (2020) The Observatory on LAkes (OLA) database: sixty years of environmental data accessible to the public. J Limnol. https://doi.org/10.4081/jlimnol.2020.1944

Rueda FJ, Fleenor WE, de Vicente I (2007) Pathways of river nutrients towards the euphotic zone in a deep-reservoir of small size: uncertainty analysis. Ecol Model 202:345–361. https://doi.org/10.1016/j.ecolmodel.2006.11.006

Schelske CL, Feldt LE, Simmons MS (1980) Phytoplankton and physical-chemical conditions in selected rivers and the coastal zone of Lake Michigan, 1972 (No. COO-2003-36). Michigan Univiversity, Ann Arbor (USA). Great Lakes Research Div. https://doi.org/10.2172/5008748

Soomets T, Kutser T, Wüest A, Bouffard D (2019) Spatial and temporal changes of primary production in a deep peri-alpine lake. Inland Waters 9:49–60. https://doi.org/10.1080/20442041.2018.1530529

Soulignac F et al (2018) Using 3D modeling and remote sensing capabilities for a better understanding of spatio-temporal heterogeneities of phytoplankton abundance in large lakes. J Great Lakes Res 44:756–764. https://doi.org/10.1016/j.jglr.2018.05.008

Soulignac F, Lemmin U, Ziabari SMH, Wynn HK, Graf B, Barry DA (2021) Rapid changes in river plume dynamics caused by advected wind-driven coastal upwelling as observed in Lake Geneva. Limnol Oceanogr 66:3116–3133. https://doi.org/10.1002/lno.11864

Sterner RW, Keeler B, Polasky S, Poudel R, Rhude K (2020) Ecosystem services of Earth's largest freshwater lakes. Ecosyst Serv 41:1010146. https://doi.org/10.1016/j.ecoser.2019.101046

Thornton KW (1990) Perspectives on reservoir limnology. In: Thornton KW, Kimmel BL, Payne FE (eds) Reservoir limnology: ecological perspectives. John Wiley & Sons, New York

van der Maarel E (1990) Ecotones and ecoclines are different. J Veg Sci 1:135–138. https://doi.org/10.2307/3236065

Vaulot D, Courties C, Partensky F (1989) A simple method to preserve oceanic phytoplankton for flow cytometric analyses. Cytometry 10:629–635. https://doi.org/10.1002/cyto.990100519

Viljanen M, Holopainen AL, Rahkola-Sorsa M, Avinsky V, Ruuska M, Leppänen S, Rasmus K, Voutilainen A (2009) Temporal and spatial heterogeneity of pelagic plankton in Lake Pyhäselkä, Finland. Boreal Environ Res 14:903–913

Woolway RI, Merchant CJ (2019) Worldwide alteration of lake mixing regimes in response to climate change. Nat Geosci 12:271–276. https://doi.org/10.1038/s41561-019-0322-x

Woolway RI, Sharma S, Weyhenmeyer GA, Debolskiy A, Golub M, Mercado-Bettín D, Perroud M, Stepanenko V, Tan Z, Grant L, Ladwig R, Mesman J, Moore TN, Shatwell T, Vanderkelen I, Austin JA, DeGasperi CL, Dokulil M, La Fuente S, Mackay EB, Schladow SG, Watanabe S, Marcé R, Pierson DC, Thiery W, Jennings E (2021) Phenological shifts in lake stratification under climate change. Nat Commun 12:2318. https://doi.org/10.1038/s41467-021-22657-4

Wüest A, Bouffard D, Guillard J, Ibelings BW, Lavanchy S, Perga M-E, Pasche N (2021) LéXPLORE: a floating laboratory on Lake Geneva offering unique lake research opportunities. Wires Water 8:e1544. https://doi.org/10.1002/wat21544

Xu FL, Tao S, Dawson RW, Li PG, Cao J (2001) Lake ecosystem health assessment: indicators and methods. Water Res 35:3157–3167. https://doi.org/10.1016/s0043-1354(01)00040-9

Yang Y, Colom W, Pierson D, Pettersson K (2016) Water column stability and summer phytoplankton dynamics in a temperate lake (Lake Erken, Sweden). Inland Waters 6:499–508. https://doi.org/10.1080/IW-6.4.874

Piton V, Soulignac F, Lemmin U, Graf B, Wynn HK, Blanckaert K, Barry DA (2022) Tracing unconfined nearfield spreading of a river plume interflow in a large lake (Lake Geneva): hydrodynamics suspended particulate matter and associated fluxes. Front Water. https://doi.org/10.3389/frwa.2022.943242